Accepted Manuscript

Iridium nanocrystals encapsulated liposomes as near-infrared light controllable nanozymes for enhanced cancer radiotherapy

Liangzhu Feng, Ziliang Dong, Chao Liang, Muchao Chen, Danlei Tao, Liang Cheng, Kai Yang, Zhuang Liu

PII: S0142-9612(18)30534-9

DOI: 10.1016/j.biomaterials.2018.07.049

Reference: JBMT 18792

To appear in: *Biomaterials*

Received Date: 11 February 2018

Revised Date: 16 July 2018

Accepted Date: 25 July 2018

Please cite this article as: Feng L, Dong Z, Liang C, Chen M, Tao D, Cheng L, Yang K, Liu Z, Iridium nanocrystals encapsulated liposomes as near-infrared light controllable nanozymes for enhanced cancer radiotherapy, *Biomaterials* (2018), doi: 10.1016/j.biomaterials.2018.07.049.

Iridium Nanocrystals Encapsulated Liposomes as Near-Infrared Light Controllable Nanozymes for Enhanced Cancer Radiotherapy

*Liangzhu Feng[1#], Ziliang Dong[1#], Chao Liang[1], Muchao Chen[1], Danlei Tao[1], Liang Cheng[1], Kai Yang[2], Zhuang Liu[1]**

Dr. L.Z. Feng, Mr. Z.L. Dong, Mr. C. Liang, Mr. M.C. Chen, Ms. D.L. Tao, Dr. L. Cheng, Prof. Z. Liu
Institute of Functional Nano & Soft Materials (FUNSOM), Jiangsu Key Laboratory for Carbon-Based Functional Materials & Devices, Soochow University, Suzhou 215123, China
[#] These authors contribute equally to this work.
*E-mail: zliu@suda.edu.cn

Dr. K. Yang
School of Radiation Medicine and Protection & School for Radiological and Interdisciplinary Sciences (RAD-X), Medical College of Soochow University, Suzhou 215123, China

Keywords: Iridium nanocrystals, thermal-responsive nanozyme, tumor hypoxia relief, NIR light, cancer radiotherapy

Abstract:

Owing to the existence of severe tumor hypoxia and limited X-ray absorption of solid tumors, the therapeutic efficacy of radiotherapy is far from satisfactory. Herein, ultrasmall iridium nanocrystals (IrNCs) with homogeneous size distribution are successfully synthesized. The obtained IrNCs show catalase-like catalytic activity towards hydrogen peroxide (H_2O_2) with great temperatures / pH stability. As free IrNCs are prone to be toxified by thiol-containing biomolecules, we encapsulate as-prepared IrNCs within stealth liposomal carriers, obtaining Ir@liposome with well-protected catalytic activity in physiological conditions. By utilizing its efficient photothermal conversion ability, such Ir@liposome shows effective near-infrared-(NIR)-responsive catalytic activity towards H_2O_2 decomposition. As revealed by *in vivo* photoacoustic imaging, our Ir@liposome exhibits efficient passive tumor accumulation upon intravenous injection, and could efficiently decompose the tumor endogenous H_2O_2 into O_2, particularly upon exposure to the NIR laser. As the results of relieved tumor hypoxia after such treatment and the radiosensitization capability of Ir as a high-Z element, greatly enhanced radio-therapeutic efficacy with Ir@liposome is then achieved. This work thus presents a unique type of NIR light controllable theranostic nanozyme based on noble metal nanocrystals as a nanoscale radiosensitizer with great performance in enhancing cancer radiotherapy.

1. Introduction

As a mainstream cancer treatment modality, radiotherapy (RT) has been demonstrated to be able to kill cancerous cells via inducing the formation of DNA breaks upon exposure to external beam radiation (*e.g.* X-rays, g-rays, electrons, *etc.*) or internal radiation from implanted radioactive isotopes [1]. Owing to the fact that oxygen is needed for the fixation of DNA breaks to enhance radiation-induced cell killing, the therapeutic efficacy of RT would be affected by the level of available oxygen molecules within the tumor [2]. However, as a result of insufficient and heterogeneous blood supply within tumors, the tumor hypoxia, that is the lack of oxygen within the tumor microenvironment, is a general feature for many types of solid tumors, and would lead to resistance of tumors to RT treatment [3]. On the other hand, tumors are soft tissues that usually have relative weak interactions with radiation beams (*e.g.* X-ray), and a large proportion of radiation energy would be imposed to adjacent normal tissues, resulting in severe side effects during RT as well as the limited therapeutic efficacy under the safe radiation dose [4].

In past decades, tremendous efforts have been devoted to looking for effective radio-sensitizing approaches for more efficient cancer RT, including concurrently applying chemotherapeutics (*e.g.* cisplatin) with RT for clinical cancer treatment [5-7]. However, the side effects of combined chemo-radiotherapy may be superimposed, causing more severe toxicities to patients compared to RT or chemotherapy alone [8-9]. Recently, with the advance of nanotechnology, tumor-homing high-Z elements containing nanomaterials that can interact and absorb radiation beams such as X-ray have been found to be a promising type of radio-sensitizer by increasing the effective dose of radiation energy applied onto the tumor to enhance radiation-induced tumor damage [10-12]. Besides, considering the negative role of tumor hypoxia in cancer RT, several different types of nanotheranostics have recently been designed to achieve more efficient RT cancer treatment by improving tumor oxygenation [13-19]. For instance, catalase, an effective enzyme that triggers the decomposition of H_2O_2 to release O_2, has recently been formulated into nanoscale platforms to relieve tumor hypoxia by decomposing the endogenous H_2O_2 (50-100 μM) existing within the tumor microenvironment, so to overcome the tumor hypoxia associated therapeutic resistance [20].

Nanozymes, which are inorganic nanostructures featured with interesting catalytic activities similar to many biological enzymes (*e.g.* peroxidase, catalase, *etc.*), have been extensively explored for cancer diagnosis and other bioapplications [21-25]. For instance, several different Ir-based

nanostructures have recently been uncovered to be efficient peroxidase / catalase mimics with great potential for biosensing and scavenging of reactive oxygen species (ROS) [26-28]. In this study, ultrasmall Ir nanocrystals (IrNCs) are synthesized via a simple chemical reduction process and encapsulated within polyethylene glycol (PEG) modified liposomes, and then employed for near-infrared (NIR) light-enhanced tumor hypoxia relief and synergistic radio-sensitization in cancer RT (**Scheme 1**). After liposomal encapsulation, the obtained Ir@liposome shows well protected and temperature-dependent catalytic activity in the physiological environment even in the presence of thiol-containing biomolecules, which are able to poison bare IrNCs. Meanwhile, owing to the stealth-like *in vivo* behaviors of PEGylated liposomes, such Ir@liposome exhibits efficient tumor accumulation owing to the enhanced permeability and retention (EPR) effect upon intravenous (i.v.) injection, as monitored by *in vivo* photoacoustic (PA) imaging via tracking the NIR absorbance of IrNCs. Notably, such Ir@liposome after tumor accumulation is able to significantly attenuate the tumor hypoxia status, particularly upon NIR laser induced mild photothermal heating to further promote the catalytic activity of such nanozyme. Owing to the greatly improved tumor oxygenation by such strategy and the capability of Ir as a high-Z element for radio-sensitization, remarkably enhanced RT treatment efficacy for tumor-bearing mice is achieved with Ir@liposome. This work thus highlights the elaborate construction of Ir-containing liposomal nanozyme with NIR light controllable catalytic activity for tumor hypoxia attenuation and radio-sensitization, promising for next generation cancer radiotherapy.

2. Experimental Section

2.1 Materials.

Sodium hexachloroiridate(III) hydrate ($Na_3IrCl_6 \cdot xH_2O$), ascorbic acid (AA), Sephadex® G-100 medium, and 3-(4,5-dimethylthiazol-2-yl)-2,5-diphenyl-tetrazolium bromide (MTT) were purchased from Sigma-Aldrich. 1,2-dipalmitoyl-snglycero-3-phosphocholine (DPPC) was purchased from Xi'an Ruixi Biological Technology Co., Ltd. PEG conjugated 1,2-distearoyl-sn-glycero-3-phosphoethanolamine (DSPE-mPEG$_{5k}$) was purchased from Laysan Bio Inc. Cholesterol was purchased from *J&K* Scientific Ltd. RPMI-1640 medium and fetal bovine serum (FBS) were purchased from Thermo Fisher Scientific Inc. Sodium borohydride ($NaBH_4$) and other chemicals were purchased from China National Pharmaceutical Group Corporation.

2.2 Synthesis and Characterization of IrNCs and Ir-GSH.

IrNCs were synthesized via a simple chemical reduction process. Briefly, 50 mL 18.2 MΩ * cm ultrapure water was added into a round-bottom flask and heated up to 95 ^{o}C before 50 mg AA and 10 mg $Na_3IrCl_6 \cdot xH_2O$ were added. Then, 25 mg $NaBH_4$ pre-dissolved in 1 mL ice-cold water was dropwisely added into the mixture under vigorous stirring for 15 min. Upon cooling down to room temperature, the IrNCs were condensed and purified by using an Amico ultrafilter device with a molecular weight cut-off (MWCO) of 10 kDa (Millipore, Bedford, MA) for further use. Ir-GSH was prepared according to the same procedure for the preparation of IrNCs, except that 20 mg glutathione (GSH) was added into the reaction mixture before stopping the heating.

The morphology of as-prepared IrNCs and Ir-GSH were observed under a transmission eletron microscopy (TEM, Tecnai F20, FEI) operated at an acceleration voltage of 200 kV. The lattice fringes of the IrNCs were observed under the high resolution TEM (Tecnai F20, FEI). The X-ray diffraction (XRD) analysis of IrNCs was performed on a Shimadzu XRD-6000 X-ray diffractometer at a scanning rate of 0.05 ° s^{-1}. The dynamic light scattering (DLS) size distribution and absorbance spectra of IrNCs were recorded using a Malvern zetasizer (nano-ZS90) and a UV-vis-NIR spectrometer (Thermo Fisher), respectively. The Ir concentration was quantified using the inductively coupled plasma mass spectrometry (ICP-MS, Aurora M90, Analytik Jena).

2.3 Preparation of Ir@liposome and Ir-GSH@liposome.

To prepare Ir@liposome and Ir-GSH@liposome, the lipid membranes were firstly prepared by dissolving DPPC, cholesterol, and DSPE-$mPEG_{5k}$ at a molar ratio of 6 : 4 : 0.5 in chloroform and then dried using a rotary evaporator. Then, the as-prepared lipid membranes were hydrated with IrNCs or Ir-GSH solutions (Ir = 5 mg mL^{-1}) at 45 ^{o}C under stirring for 30 min, followed by being extruded through a 200 nm polycarbonate filters at 45 °C for 20 times. Afterwards, those unencapsulated IrNCs or Ir-GSH were removed by running through a sephadex G-100 column with PBS as the mobile phase, and condensed with an Amico ultrafilter device with a MWCO of 100 kDa.

2.4 Catalase-Like Activity Assay.

The catalase-like activity assays were performed at 37 ^{o}C using the Góth method [29]. To evaluate its Michaelis-Menten constant (K_m), 200 μL of the as-prepared IrNCs solution (20 μg mL^{-1})

was added into 1 mL pre-warmed phosphate buffer solution (67 mM) containing H_2O_2 and kept at 37 ^oC for 1 min. Then, 1 mL ammonium molybdate solution (Mo = 240 mM) was rapidly added into the reaction mixture with its absorbance at 405 nm measured using a UV-vis spectrometer. The K_m of IrNCs was calculated using the Lineweaver-Burk plot. Besides, the K_m of catalase was measured using the same procedure at the catalase concentration of 1 μg mL^{-1}.

Then, the thermal and pH stabilities of IrNCs towards H_2O_2 decomposition were carefully studied and compared with that of catalase. In brief, IrNCs and catalase (0.1 mg mL^{-1}) were pre-incubated at 80 ^oC for different time intervals or incubated at varying pH values for 2 h, and their catalytic activities were then measured by using the aforementioned Góth method with a fixed H_2O_2 concentration of 50 mM at 37 ^oC. In addition, the effect of temperature on the catalytic activity enhancement of as-prepared IrNCs and catalase were carefully studied by measuring their catalytic activities at 25, 37, 45, and 60 ^oC by following the aforementioned Góth method with a fixed H_2O_2 concentration of 50 mM. The relative catalytic activities of IrNCs or catalase were obtained by normalizing the obtained catalytic activities of each sample under varying reaction temperatures to the one measured at 25 ^oC.

Afterwards, the catalytic activities of as-prepared IrNCs, Ir-GSH, Ir@liposome, and Ir-GSH@liposome (Ir = 5 μg mL^{-1}) were further evaluated by recording their oxygen generation capacities when incubated with H_2O_2 solutions (1 mM) using a portable dissolved oxygen meter. Besides, the photothermal effect of IrNCs on their catalytic activity was studied by recording the oxygen generation from the H_2O_2 solution (1 mM) in the presence of IrNCs (10 μg mL^{-1}) upon being exposed to a 785-nm laser at a power density of 1 W cm^{-2}.

2.5 In vitro Cell Viability Assay.

4T1 murine breast cancer cells were maintained according to the recommended procedure. For cell viability assay, 4T1 cells seeded in 96-well plates were incubated with Ir@liposome or Ir-GSH@liposome at a series of Ir concentrations for 24 h, followed by the standard MTT cell viability assay.

2.6 In vitro Clonogenic Survival Assay.

For clonogenic survival assay, different numbers of 4T1 cells were seeded in 6-well plates and cultured at 37 ^oC overnight. Then, these cells were incubated with Ir@liposome or

Ir-GSH@liposome (Ir = 50 μg mL^{-1}) under the hypoxic condition (5% CO_2 / 1% O_2 / 94% N_2) for 12 h to induce hypoxic phenotype according to the previously reported method [30]. Then, those cells were exposed to an X-ray Irradiator (RS-2000, RAD source, photon energy = 140 keV) at doses of 0, 2, 4 or 6 Gy. The cells of control group were treated under the same parameters in the absence of Ir@liposome or Ir-GSH@liposome. After 1 h, cells were washed with PBS and cultured in fresh medium at 37 °C under the normoxic condition for another 7 days. After that, those cells were fixed with methanol and stained with Giemsa solution for surviving fraction statistics according to the standard method.

2.7 In vitro Immunofluorescence Staining of γ-H_2AX.

To evaluate the DNA damage post different treatments under a hypoxic condition, the double strand break status of those 4T1 cells were visualized using a confocal microscopy (SP5II, Leica) by recording the fluorescence signals of γ-H_2AX, a well-known marker of DNA double stand break, following the literature protocol [20]. Briefly, 4T1 cells were incubated with Ir@liposome or Ir-GHS@liposome at an Ir concentration of 50 μg mL^{-1} under the hypoxic condition for 12 h, followed by being subjected to X-ray exposure at a dose of 6 Gy. After another 1 h incubation at 37 ^oC, those cells were washed with PBS, fixed with 4% paraformaldehyde, and stained with anti-phospho-histone γ-H_2AX mouse monoclonal antibody and 4,6-diamino-2-phenyl indole (DAPI) according to the procedure provided by the manufacturer. Finally, the cells were imaged by using a confocal microscopy. Quantitative analysis of γ-H_2AX foci density (foci/100 μm^2) was conducted automatically using the ImageJ software for 100 cells in each treatment group.

2.8 Tumor Models.

Female Balb/c mice mice of 18~20 g were purchased from Nanjing Sikerui Biological Technology Co. Ltd. and used under protocols approved by the laboratory animal center of Soochow University. For 4T1 tumor model inoculation, 2×10^6 4T1 cells suspended in 50 μL PBS were subcutaneously injected to the back of each mouse. The mice were used when the tumor volumes reached ~100 mm^3.

2.9 PA Imaging with Ir@liposome.

To study the correlations between PA signal intensities and Ir concentrations, Ir@liposome was

suspended in Matrigel (Corning) to different concentrations and the final concentration of Matrigel was 50% v/v for all solutions. Then, the Matrigel mixtures (50 μL) were injected subcutaneously on the dorsal aspects of female nude mice to measure their corresponding PA signals using the Visualsonic Vevo® 2100 LAZER system with an excitation wavelength of 732 nm. For *in vivo* PA imaging, 4T1 tumor-bearing mice were anesthetized and then *i.v.* injected with Ir@liposome at an Ir dose of 6 mg kg^{-1}. At difference time intervals post injection, the tumor region was imaged using the Visualsonic Vevo® 2100 LAZER system with an excitation wavelength of 732 nm.

2.10 In vivo Pharmacokinetics Study of Ir@liposome.

To evaluate the blood circulation profile, three healthy mice were i.v. injected with Ir@liposome at a dose of 6 mg kg^{-1} in terms of Ir. Then, ~20 μL blood samples were withdrawn from each mouse at different time intervals post injection. After that, the Ir concentration of each blood sample was measured using an ICP-MS after being dissolved with aqua regia. For the evaluation of biodistribution profile, three tumor bearing mice received an i.v. injection of Ir@liposome at an Ir dose of 6 mg kg^{-1}. After 24 h, those mice were sacrificed with their main organs collected, weighted, and dissolved using aqua regia. Thereafter, their Ir concentrations were measured using an ICP-MS.

2.11 In vivo Tumor Hypoxia Evolution.

Ex vivo immunofluorescence staining assay was utilized to study tumor hypoxia evolution of those mice with injection of Ir@liposome. Briefly, a total of 15 mice bearing 4T1 tumors were divided into 5 groups (n = 3 mice per group) as follows: two groups of mice were i.v. injected with Ir@liposome, another two groups of mice were i.v. injected with Ir-GSH@liposome, and the other group of mice received an i.v. injection of saline as the negative control. The Ir doses for both Ir@liposome and Ir-GSH@liposome injection were 6 mg kg^{-1}. At 24 h p.i., two groups of mice with injection of Ir@liposome and Ir-GSH@liposome were irradiated by a 785-nm laser (0.8 W cm^{-2}) with tumor temperature controlled at ~45 ^{o}C according to a thermal camera (Fotric 225) for 20 min. Later, all mice were intraperitoneally (i.p.) injected with pimonidazole hydrochloride (Hypoxyprobe^{TM}, USA) at a dose of 30 mg kg^{-1} according to the procedure provided by the manufacturer. 90 min post injection of pimonidazole hydrochloride, the mice were sacrificed to collect frozen tumor slices for immunofluorescence staining to visualize the fluorescent hypoxia

signals from pimonidazole by adopting our previously used procedure [31]. Moreover, the expression levels of HIF-1α proteins in those tumor slices post various treatments were also stained according to the immunofluorescence staining procedures provided by the manufacture. Finally, the hypoxia region of each slice was statistically analyzed using the Image-J software according to the previously used procedures.

2.12 In vivo Treatment.

35 tumor bearing mice were randomly divided into 7 groups (5 mice per group), and received following treatments when the tumor size reaching ~100 mm^3: (I) control group with saline injection only; (II) bare RT group with saline injection plus X-ray exposure; (III) Ir-GSH@liposome injection plus X-ray exposure; (IV) Ir@liposome injection only; (V) Ir@liposome injection plus X-ray exposure, (VI) Ir@liposome injection plus 785 nm laser irradiation, and (VII) Ir@liposome injection plus sequential 785 nm laser irradiation and X-ray exposure. The dose of Ir was 6 mg kg^{-1}. At 24 h p.i., the mice in group (II), (III), (V), (VI), and (VII) were exposed to the 785-nm laser (0.8 W cm^{-2} for 20 min, tumor temperature controlled at ~45 ^oC), or X-ray radation at the dose of 6 Gy, or both for group (VII). Since the beginning of the treatment, the size of each tumor was recorded by measuring its length (*L*) and width (*W*) using a digital caliper every two days. The tumor volume (*V*) was calculated by the following equation: $V = LW^2/2$. Moreover, the therapeutic effects of those different treatments were further evaluated using the terminal deoxynucleotidyl transferase dUTP nick end labeling (TUNEL) assay.

3. Results and Discussion

In this work, IrNCs were synthesized via a simple chemical reduction process from their precursor, sodium hexachloroiridate(III) hydrate ($Na_3IrCl_6 \cdot xH_2O$), with ascorbic acid (AA) as the capping agent and sodium borohydride ($NaBH_4$) as the reducing agent after heating at 95 ^oC for 15 min (**Figure 1a**). After detailed screening, it was found that the IrNCs prepared by mixing $Na_3IrCl_6 \cdot xH_2O$, AA and $NaBH_4$ at the mass feeding ratio of 1 : 5 : 2.5 showed excellent stability in water and saline. Under transmission electron microscopy (TEM), the as-prepared IrNCs showed homogenous size distribution with a mean size of ~3.3 nm (**Figure 1b, supporting Figure S1**). The lattice spacing of such IrNCs was measured to be ~0.22 nm as observed by the high resolution TEM

(**Figure 1b, inset**), indicating the crystalline face-centered cubic (fcc) of IrNCs, which was further confirmed by the X-ray diffraction (XRD) analysis (**Figure 1c**).

After that, the steady-state kinetics of such IrNCs towards H_2O_2 decomposition was studied by measuring the initial rates as a function of H_2O_2 concentration using the Góth method [29]. It was found that the catalytic property of such IrNCs followed typical Michiaelis-Menten (MM) model. As determined by the corresponding Lineweaver-Burk plots (**Supporting Figure S2a&b**), the MM constant (K_m) was calculated to be ~132 mM, a little higher than that of catalase (~50.6 mM) (**Supporting Figure S2c&d**), consistent with those previous reports [26]. Then, the thermal and pH stabilities of such IrNCs were carefully studied via the Góth method. It was uncovered that the catalytic activity of IrNCs showed much less fluctuation after being incubated at 80 ^{o}C for 2 h compared to that of catalase (**Supporting Figure S2e**). Besides, unlike catalase which showed dramatically dropped catalytic activity under acidic pH, our IrNCs retained a high level of catalytic activity within a large pH range (**Supporting Figure S2f**). Therefore, IrNCs as a nanozyme exhibit much higher thermal and pH stability compared to its biological enzyme counterpart, catalase.

The catalytic capacity of IrNCs towards H_2O_2 decomposition was further evaluated by recording the oxygen generation using a portable dissolved oxygen meter. It was found that our IrNCs (Ir = 5 μg mL^{-1}) induced effective oxygen generation within H_2O_2 solutions (**Figure 1d**). However, the catalytic activity of those bare as-made IrNCs would be significantly suppressed in the presence of thiol-containing biomolecules such as glutathione (GSH) and bovine serum albumin (BSA), which would toxify nanozyme IrNCs likely owing to the reaction between thiol groups and the active sites on the surface of IrNCs [32, 33]. For instance, GSH mixed IrNCs (Ir-GSH) showed similar morphology and size distribution to those of bare IrNCs (**Supporting Figure S3a&b**), while their catalytic activity towards H_2O_2 decomposition nearly disappeared (**Supporting Figure S3c**). Owing to the wide existence of thiol-containing molecules in the physiological environment, bare as-made IrNCs thus cannot be directly used in biological systems.

To confer IrNCs excellent catalytic stability in physiological environments (*e.g.* in the presence of thiol-containing biomolecules) and efficient tumor homing capacity, the as-prepared ultrasmall IrNCs were encapsulated within the aqueous cavities of PEGylated liposomes, which are well-known for their great biocompatibility and versatile role in molecular loading [31, 34-36]. In our experiments, the Ir@liposome sample was obtained by hydrating the lipid membrane of DPPC, cholesterol, and DSPE-$mPEG_{5k}$ at a molar ratio of 6 : 4 : 0.5, by an aqueous solution of IrNCs. As

revealed under TEM imaging, such Ir@liposome nanoparticles were found to show spherical morphology, with multiple ultra-small individual IrNCs encapsulated within one liposomal nanoparticle (**Figure 1e**). Moreover, by utilizing the high resolution TEM imaging, the lattice spacing of the encapsulated IrNCs was determined to be ~0.22 nm, which was same as that of as-prepared IrNCs (**Figure 1e, insert**). As determined by dynamic light scattering (DLS), Ir@liposome nanoparticles showed a mean hydrodynamic size of ~100 nm, which appeared to be much larger than that of bare IrNCs at ~10 nm (**Figure 1f**). By using the thermogravimetric analysis (TGA), the loading capacity of IrNCs within Ir@liposome nanoparticles was determined to be 15.6% by weight (**Supporting Figure S4**). Our results collectively indicate the successful encapsulation of IrNCs within liposomes. More interestingly, unlike IrNCs whose catalytic function could be greatly suppressed in the presence of thiol-containing molecules (**Figure 1d**), the obtained Ir@liposome (Ir = 5 μg mL^{-1}) could trigger efficient H_2O_2 decomposition even in the presence of BSA or FBS (**Figure 1g, supporting Figure S5**). Such a well-protected catalytic activity of Ir@liposome towards H_2O_2 decomposition should be ascribed to the efficient shielding effect of the liposome shell to prevent the direct contact between thiol-containing proteins with IrNCs.

As measured by the UV-Vis-NIR spectrometer, Ir@liposome showed efficient optical absorption in the NIR region, similar to bare IrNCs (**Figure 2a**), which had a mass extinction coefficient of 12.5 mL mg^{-1} cm^{-1} at 785 nm (**Supporting Figure S6**). Then, upon exposure to 785 nm laser, it was found that the temperatures of Ir@liposome solution (Ir = 10 μg mL^{-1}) showed laser-power-density dependent rapid increase (**Figure 2b**), indicating the efficient photothermal conversion of IrNCs. By using the Góth method, it was found that catalytic activities of Ir@liposome (Ir = 4 μg mL^{-1}) towards H_2O_2 decomposition showed significant increase as the rise of solution temperatures, while free catalase showed minimal increase of its catalytic activity when measured at elevated temperatures (**Figure 2c**). Such a significant temperature dependent catalytic activity of Ir@liposome towards H_2O_2 decomposition is speculated to be ascribed to increased molecular motion under the elevated temperature, which would speed up the interaction between H_2O_2 and IrNCs in accordance with those previous reports [23, 26]. Besides, as measured by the portable dissolved oxygen meter, we found that H_2O_2 solutions added with Ir@liposome (Ir = 5 μg mL^{-1}) showed effective temperature dependent oxygen generation (**Figure 2d**). More interestingly, it was further uncovered that the rate of oxygen generation from H_2O_2 solutions in the presence of Ir@liposome (Ir = 10 μg mL^{-1}) could be significantly speeded up upon exposure to the 785-nm NIR

laser irradiation at a power density of 1 W cm^{-2} (**Figure 2e**), owing to the photothermal heating effect of IrNCs. Therefore, the photothermal conversion ability of Ir@liposome could be utilized to remotely control its catalytic activity towards H_2O_2 decomposition, demonstrating it to be a promising NIR-controllable nanozyme (**Figure 2f**).

Next, we ought to study the radio-sensitizing effect of Ir@liposome at the *in vitro* level. Ir-GSH@liposome, which was prepared by replacing bare IrNCs with Ir-GSH following the same liposome preparation procedure, was used as the negative control of Ir@lipsome (**Supporting Figure S3b**). Both two types of Ir-containing liposomes exhibited no appreciable toxic effects towards 4T1 breast cancer cells within our tested concentration ranges (**Figure 3a**). Then, the capability of Ir@liposome on sensitizing RT was carefully evaluated. From the clonogenic survival assay results, it was found that 4T1 cells treated with Ir@liposome (Ir = 50 μg mL^{-1}) followed by X-ray irradiation (photon energy = 140 keV, doses = 2, 4, and 6 Gy) under a hypoxic incubation condition (1% O_2 / 94% N_2 / 5% CO_2) showed obviously reduced viable clone formation compared with those treated with Ir-GSH@liposome (**Figure 3b**). Furthermore, based on the immunofluorescence staining of γ-H_2AX, a classic marker of double-strand DNA breaks [20], we found that the cells treated with Ir@liposome plus X-ray exposure showed the highest level of DNA damages compared to the other control groups (**Figure 3c&d**). Notably, although less effective compared to Ir@lipsome, Ir-GSH@liposome also exhibited significant radio-sensitizing effect to enhance the *in vitro* RT efficacy, owing the high X-ray attenuation coefficient of Ir as a high-Z element. Therefore, the effective RT enhancing function of Ir@liposome is attributed to both the radio-sensitizing effect of Ir, as well as the ability of IrNCs to enable intracellular re-oxygenation via triggering decomposition of H_2O_2 produced by tumor cells [20].

With strong NIR optical absorption, Ir@liposome could thus be tracked under photoacoustic (PA) imaging, an emerging optical-sound imaging modality by detecting ultrasound signals generated from the absorbed pulsed laser energy as the result of photothermal expansion [37-39]. Upon subcutaneous injection of Ir@liposome premixed with Matrigel, it was found that our Ir@liposome showed a concentration-dependent PA signal enhancement with a rather low detection threshold of ~5 μg mL^{-1} under the Visualsonic Vevo 2100 LAZER PA imaging system (**Figure 4a**). The PA signal intensities of Ir@liposome were found to show a linear proportional to its concentrations (R^2 = 0.997) (**Figure 4b**). We then used PA imaging to track *in vivo* tumor retention of Ir@liposome. Mice bearing 4T1 tumors were intravenously (i.v.) injected with Ir@liposome (Ir =

6 mg kg^{-1}) and imaged under the PA imaging system. Gradually increased PA signals were observed within the tumor post injection of Ir@liposome (**Figure 4c**), suggesting the efficient tumor retention of those Ir@liposome nanoparticles. By semi-quantitative analysis, it was uncovered that the PA signals in the tumor increased over time and approached the saturation level at ~8 h post injection (p.i.) (**Supporting Figure S7**).

Moreover, the detailed pharmacokinetic profiles of such Ir@liposome were carefully studied by recording the Ir concentrations using the inductively coupled plasma mass spectrometry (ICP-MS). It was found that the blood circulation of Ir@liposome followed a typical two-compartment mode, with the first half-life ($t_{1/2(\alpha)}$) and second half-life ($t_{1/2(\beta)}$) measured to be 0.95 ± 0.04 h and 17.0 ± 0.96 h, respectively (**Figure 4d**). Additionally, the tumor accumulation of Ir@liposome was measured to be 4.6 ± 0.65% ID g^{-1} (percentage of injected dose per gram tissue) at 24 h p.i. Moreover, high accumulations of Ir@liposome were also found in the liver and spleen (**Figure 4e**), the reticuloendothelial systems (RES) to clear foreign nanoparticles. Taken together, all these results demonstrate that Ir@liposome nanoparticles with stealth-like long blood circulation time would show efficient tumor retention owing to the EPR effect.

Next, the tumor hypoxia status post i.v. injection of the Ir@liposome was carefully studied via the *ex vivo* immunofluorescence staining with Pimonidazole as the exogenous hypoxia staining probe and hypoxia induced factor 1α (HIF-1α) protein as the endogenous hypoxia reporter, respectively, following the standard protocols. Based on preliminary study indicating that Ir@liposome showed most effective tumor hypoxia attenuation at 24 h post i.v. injection (data no shown), a total of 15 mice bearing 4T1 tumors with a size of 100 mm^3 were randomly divided to 5 groups, with two groups of mice i.v. injected with Ir@liposome and the other two groups of mice i.v. injected with Ir-GSH@liposome at the same Ir dose of 6 mg kg^{-1}. At 24 h post injection of nanoparticles, two groups of mice with corresponding i.v. injection of Ir@liposome and Ir-GSH@liposome were subjected to 785 nm laser irradiation (0.8 W cm^{-2}) for 20 min with the temperature of tumors controlled at ~45 ^{o}C (**Supporting Figure S8**), as monitored by a thermal camera (Fotric 225), while the other three groups of mice were not exposed to the laser irradiation. Interestingly, tumors on mice with i.v. injection of Ir@liposome showed remarkably decreased hypoxia signals, which were further attenuated upon 785 nm laser irradiation. In contrast, i.v. injection of Ir-GSH@liposome with the GSH-poisoned nanozyme resulted in much less significant change of the tumor hypoxia status, even with NIR laser irradiation (**Figure 5a**). By

semi-quantitative analysis of the hypoxia positive signals in those tumor slices, it was uncovered that the percentages of hypoxia positive area dropped from ~46.6% for the control tumor, to ~23.4% and ~8.3% for those collected from the mice with *i.v.* injection of Ir@liposome in absence or presence of 785-nm laser irradiation, respectively (**Figure 5b**). In comparison, for mice with i.v. injection of Ir-GSH@liposome, only a slight drop of hypoxia positive area (to ~34.4%) in their tumors was observed for those receiving 785-nm laser irradiation. Similarly, by analyzing the expression levels of HIF-1α in those tumor slices, we found that i.v. injection of Ir@liposome plus 785-nm laser irradiation could lead to the most efficient down-regulation of HIF-1α, while i.v. injection of Ir-GSH@liposome showed only a minor effect to the HIF-1α expression even with laser exposure (**Supporting Figure S9**). These results collectively indicate that our Ir@liposome could efficiently relieve tumor hypoxia upon irradiation by a NIR laser, owing to the photothermally enhanced nanozyme activity of such Ir@liposome to decompose tumor endogenous H_2O_2 and promote tumor oxygenation.

Finally, we evaluated the *in vivo* RT enhancing effect of such Ir@liposome on 4T1 tumor bearing mice. A total of 35 female Balb/c mice bearing 4T1 tumors at the initial sizes of ~100 mm^3 were randomly divided into seven groups (n = 5 per group) as follows: (I) control group with saline injection only; (II) bare RT group with saline injection plus X-ray exposure; (III) Ir-GSH@liposome injection plus X-ray exposure; (IV) Ir@liposome injection only; (V) Ir@liposome injection plus X-ray exposure, (VI) Ir@liposome injection plus 785-nm laser irradiation, and (VII) Ir@liposome injection plus sequential 785-nm laser irradiation and X-ray exposure. The Ir dose for Ir@liposome and Ir-GSH@liposome injection was 6 mg kg^{-1}, the laser power density was ~0.8 W cm^{-2} with tumor temperature controlled at ~45 ^oC for 20 min, while the X-ray radiation was applied at a dose of 6 Gy (photon energy = 140 keV). Both NIR laser and X-ray treatments were conducted at 24 h p.i. in the corresponding groups because at this time point those tumors with Ir@liposome injection showed the most effective tumor hypoxia attenuation. Then, the tumor sizes were recorded using a digital caliper. It was found that the treatment of Ir@liposome injection plus sequential 785 nm laser irradiation and X-ray exposure (Group VII) showed the most effective tumor growth suppression among all other treatment groups (**Figure 5c**), while NIR laser irradiation of tumors on mice injected with Ir@liposome could only partly delay the tumor growth under the current mild photothermal heating conditions. Notably, In fact, tumors on 3 of 5 mice in Group VII were completely disappeared after treatment for up to 21 days (**Supporting Figure S10**). Besides, it was

found that the treatment of Ir@liposome injection plus X-ray exposure (Group V) was more effective in inhibiting the tumor growth compared to the treatment of Ir-GSH@liposome injection plus X-ray exposure (Group III), while the latter treatment only showed a slight therapeutic enhancement effect for RT cancer treatment (Group II) under the relatively low Ir injection dose.

To further evaluate the therapeutic efficacy, the apoptosis levels of tumors collected at day 4 post various treatments were examined by the terminal deoxynucleotidyl transferase dUTP nick end labeling (TUNEL) assay. It was found that the tumor slice taken from mice with Ir@liposome injection plus sequential laser irradiation and X-ray exposure exhibited the highest level of apoptosis, while only moderate levels of apoptosis were observed on the slices collected from the mice with other treatments (**Figure 5d**), following the same trend of tumor growth data (**Figure 5c**). Taken together, our results demonstrate that Ir@liposome could act as a NIR light controllable liposomal nanozyme for effective RT enhancement, not only by efficiently relieve tumor hypoxia via IrNC-mediated NIR-enhanced decomposition of tumor endogenous H_2O_2, but also by utilizing the high X-ray attenuation coefficient of Ir.

Moreover, we also studied the biocompatibility of such Ir@liposome at the *in vivo* level. By recording the body weights of each group of mice, it was found that the i.v. injection of Ir@liposome under the tested dose showed negligible influence on the body weights of those mice throughout the whole treatment period (**Figure S11a**). Additionally, at 14 day post the treatment, hematoxylin and eosin (H&E) staining of main organ slices collected from mice with Ir@liposome injection did not show any obvious histological damage in comparison with those collected from saline injected mice (**Figure S11b**), even though a relative high accumulation of Ir@liposome in liver and spleen was observed at 24 h p.i. (**Figure 3d**). Therefore, our results preliminarily demonstrated that Ir@liposome at our treatment dose could be a safe nano-theranostic agent.

In this work, IrNCs-encapsulated liposomes were prepared and utilized as an efficient NIR light controllable catalase mimic as well as a high-Z element based radio-sensitizer for synergistic cancer radiotherapy. Although IrNCs have been reported to be an efficient catalase mimic, their *in vivo* applications for cancer therapy have rarely been explored. As the catalytic activity of naked IrNCs could be toxified by thiol-containing biomolecules, we thus encapsulated IrNCs within PEGylated liposomes, which not only offered effective protection for the IrNC catalytic activity, but also enabled long-term blood circulation and effective tumor passive retention of IrNCs (**Figure 1,**

Figure 4). Moreover, like many other nanozymes, our Ir@liposome showed superior temperature / pH stability towards H_2O_2 decomposition to its biological counterpart, catalase [7, 20].

Photothermal heating has been widely explored and utilized as a non-invasive approach for effective cancer photothermal therapy and controllable drug delivery with high spatial / temporal resolution [40]. Utilizing its intrinsic NIR absorbance (**Figure 2a**), the obtained Ir@liposome showed efficient photothermal heating effect (**Figure 2d**). Owing to the temperature-dependent catalytic activity of IrNCs, such Ir@liposome exhibited intriguing NIR-controllable catalytic activity towards H_2O_2 decomposition (**Figure 2e**). Therefore, with efficient tumor retention, our Ir@liposome could effectively enhance tumor oxygenation by decomposing tumor endogenous H_2O_2 upon NIR laser irradiation of those tumors.

As for radio-sensitization, it has been widely demonstrated that tumor-homing high-Z element containing nanostructures (*e.g.* gold nanostructures) are able to improve radiation-induced tumor destruction by depositing X-ray energy within the tumor, and therefore would lead to enhanced radiotherapy efficacy under reduced radiation doses [21]. As a high-Z element, Ir within Ir@liposome could act as a radio-sensitizer. Such effect together with the NIR-triggered tumor hypoxia relief function would make Ir@liposome a rather effective nano-agent to remarkably enhance the therapeutic outcome of radiotherapy towards solid tumors. Moreover, considering the clinic use of iridium-192 as the implants for brachytherapy [41], as well as no appreciable *in vivo* side effects observed in our experiments (**Figure S11**), our Ir@liposome may indeed be a promising radio-sensitizing agent for potential clinical use.

4. Conclusion

In summary, a unique type of noble-metal-nanocrystal-encapsulated liposomes is prepared in this work and utilized as an efficient NIR light controllable catalase mimic as well as a high-Z element based radio-sensitizer for synergistic RT sensitization. After encapsulating IrNCs into liposomes, the obtained Ir@liposome exhibits well-protected catalase-like activity, as well as stealth-like long blood circulation time to enable efficient retention in tumors on mice after systemic administration, as vividly revealed by *in vivo* PA imaging. Upon NIR light irradiation, Ir@liposome would show increased catalase-like catalytic activity to trigger decomposition of tumor endogenous H_2O_2 and improved tumor oxygenation, which together with the intrinsic radio-sensitizing function of Ir as a high-Z element would enable remarkably enhanced cancer radiotherapy. Therefore, our

work presents an intriguing type of nanozyme whose catalytic activity could be remotely controlled by NIR light. Such nanozyme with multiple functionalities appears to be particularly promising for imaging-guided, synergistically enhanced RT treatment of cancer.

Supporting Information

Figures S1-S10 can be found in the supporting information.

Acknowledgements

This work was partially supported by the National Natural Science Foundation of China (51525203, 51761145041), the National Research Programs from the Ministry of Science and Technology (MOST) of China (2016YFA0201200), the China Postdoctoral Science Foundation (2017M610348, 2018T110545), the Collaborative Innovation Center of Suzhou Nano Science and Technology, the 111 Program from the Ministry of Education of China, and a Project Funded by the Priority Academic Program Development (PAPD) of Jiangsu Higher Education Institutions.

References:

[1] Brown JM, Wilson WR. Exploiting tumour hypoxia in cancer treatment. Nat. Rev. Cancer 4 (2004) 437-447.

[2] Moeller BJ, Richardson RA, Dewhirst MW. Hypoxia and radiotherapy: opportunities for improved outcomes in cancer treatment. Cancer Metast. Rev. 26 (2007) 241-248.

[3] Vaupel P, Mayer A. Hypoxia in cancer: significance and impact on clinical outcome. Cancer Metast. Rev. 26 (2007) 225-239.

[4] Dreaden EC, Mackey MA, Huang X, Kang B, El-Sayed MA. Beating cancer in multiple ways using nanogold. Chem. Soc. Rev. 40 (2011) 3391-3404.

[5] Garcia-Barros M, Paris F, Cordon-Cardo C, Lyden D, Rafii S, Haimovitz-Friedman A, et al. Tumor response to radiotherapy regulated by endothelial cell apoptosis. Science 300 (2003)1155-1159.

[6] Song G, Cheng L, Chao Y, Yang K, Liu Z. Emerging Nanotechnology and Advanced Materials for Cancer Radiation Therapy. Adv. Mater. 29 (2017) 1700996 -1701020.

[7] Zhang R, Song X, Liang C, Yi X, Song G, Chao Y, et al. Catalase-loaded cisplatin-prodrug-constructed liposomes to overcome tumor hypoxia for enhanced chemo-radiotherapy of cancer. Biomaterials 138 (2017)13-21.

[8] Bonner JA, Harari PM, Giralt J, Cohen RB, Jones CU, Sur RK, et al. Radiotherapy plus cetuximab for locoregionally advanced head and neck cancer: 5-year survival data from a phase 3 randomised trial, and relation between cetuximab-induced rash and survival. Lancet Oncol. 11 (2010) 21-28.

[9] Adelstein DJ, Li Y, Adams GL, Jr HW, Kish JA, Ensley JF, et al. An Intergroup Phase III Comparison of Standard Radiation Therapy and Two Schedules of Concurrent Chemoradiotherapy in Patients With Unresectable Squamous Cell Head and Neck Cancer. J. Clin. Oncol. 21 (2003) 92-98.

[10] Hainfeld JF, Slatkin DN, Smilowitz HM. The use of gold nanoparticles to enhance radiotherapy in mice. Phys. Med. Biol. 49 (2004) N309-N315.

[11] Song G, Liang C, Yi X, Zhao Q, Cheng L, Yang K, et al. Perfluorocarbon‐Loaded Hollow Bi2Se3 Nanoparticles for Timely Supply of Oxygen under Near‐Infrared Light to Enhance the Radiotherapy of Cancer. Adv. Mater. 28 (2016) 2716-2723.

[12] Fan W, Shen B, Bu W, Chen F, Zhao K, Zhang S, et al. Rattle-structured multifunctional nanotheranostics for synergetic chemo-/radiotherapy and simultaneous magnetic/luminescent dual-mode imaging. J. Am. Chem. Soc. 135 (2013) 6494-6503.

[13] Abbasi AZ, Gordijo CR, Amini MA, Maeda A, Rauth AM, DaCosta RS, et al. Hybrid Manganese Dioxide Nanoparticles Potentiate Radiation Therapy by Modulating Tumor Hypoxia. Cancer Res. 76 (2016) 6643-6656.

[14] Song G, Liang C, Gong H, Li M, Zheng X, Cheng L, et al. Core–Shell MnSe@Bi2Se3 Fabricated via a Cation Exchange Method as Novel Nanotheranostics for Multimodal Imaging and Synergistic Thermoradiotherapy. Adv. Mater. 27 (2015) 6110-6117.

[15] Liu J-n, Bu W, Shi J. Chemical design and synthesis of functionalized probes for imaging and treating tumor hypoxia. Chem. Rev. 117 (2017) 6160-6224.

[16] Gordijo CR, Abbasi AZ, Amini MA, Lip HY, Maeda A, Cai P, et al. Design of Hybrid MnO2-Polymer-Lipid Nanoparticles with Tunable Oxygen Generation Rates and Tumor Accumulation for Cancer Treatment. Adv. Funct. Mater. 25 (2015)1858-1872.

[17] Song X, Feng L, Liang C, Yang K, Liu Z. Ultrasound Triggered Tumor Oxygenation with Oxygen-Shuttle Nanoperfluorocarbon to Overcome Hypoxia-Associated Resistance in Cancer Therapies. Nano Lett. 16 (2016) 6145-6153.
[18] Chen Q, Feng L, Liu J, Zhu W, Dong Z, Wu Y, et al. Intelligent Albumin–MnO2 Nanoparticles as pH-/H2O2-Responsive Dissociable Nanocarriers to Modulate Tumor Hypoxia for Effective Combination Therapy. Adv. Mater. 28 (2016) 7129-7136.
[19] Cheng Y, Cheng H, Jiang C, Qiu X, Wang K, Huan W, et al. Perfluorocarbon nanoparticles enhance reactive oxygen levels and tumour growth inhibition in photodynamic therapy. Nat. Commun. 6 (2014) 8785-8795.
[20] Song G, Chen Y, Liang C, Yi X, Liu J, Sun X, et al. Catalase-Loaded TaOx Nanoshells as Bio-Nanoreactors Combining High-Z Element and Enzyme Delivery for Enhancing Radiotherapy. Adv. Mater. 28 (2016) 7143-7148.
[21] Yang X, Yang M, Pang B, Vara M, Xia Y. Gold Nanomaterials at Work in Biomedicine. Chem. Rev. 115 (2015) 10410-10488.
[22] Wei H, Wang E. Nanomaterials with enzyme-like characteristics (nanozymes): next-generation artificial enzymes. Chem. Soc. Rev. 42 (2013) 6060-6093.
[23] Fan J, Yin J-J, Ning B, Wu X, Hu Y, Ferrari M, et al. Direct evidence for catalase and peroxidase activities of ferritin–platinum nanoparticles. Biomaterials 32 (2011) 1611-1618.
[24] Zhang W, Hu S, Yin J-J, He W, Lu W, Ma M, et al. Prussian blue nanoparticles as multienzyme mimetics and reactive oxygen species scavengers. J. Am. Chem. Soc. 138 (2016) 5860-5865.
[25] Gao L, Zhuang J, Nie L, Zhang J, Zhang Y, Gu N, et al. Intrinsic peroxidase-like activity of ferromagnetic nanoparticles. Nat. Nanotechnol. 2 (2007) 577-583.
[26] Su H, Liu D-D, Zhao M, Hu W-L, Xue S-S, Cao Q, et al. Dual-enzyme characteristics of polyvinylpyrrolidone-capped iridium nanoparticles and their cellular protective effect against H2O2-induced oxidative damage. ACS Appl. Mater. Interfaces 7 (2015) 8233-8242.
[27] Xia X, Zhang J, Lu N, Kim MJ, Ghale K, Xu Y, et al. Pd–Ir core–shell nanocubes: a type of highly efficient and versatile peroxidase mimic. ACS Nano 9 (2015) 9994-10004.
[28] Ye H, Yang K, Tao J, Liu Y, Zhang Q, Habibi S, et al. An Enzyme-Free Signal Amplification Technique for Ultrasensitive Colorimetric Assay of Disease Biomarkers. ACS Nano. 11 (2017) 2052-2059.
[29] Goth L. A simple method for determination of serum catalase activity and revision of reference range. Clin. Chim. Acta 196 (1991) 143-151.
[30] Sørensen BS, Alsner J, Overgaard J, Horsman MR. Hypoxia induced expression of endogenous markers in vitro is highly influenced by pH. Radiother. Oncol. 83 (2007) 362-366.
[31] Feng L, Cheng L, Dong Z, Tao D, Barnhart TE, Cai W, et al. Theranostic Liposomes with Hypoxia-Activated Prodrug to Effectively Destruct Hypoxic Tumors post Photodynamic Therapy. ACS Nano 11 (2016) 927-937.
[32] Dong J, Song L, Yin J-J, He W, Wu Y, Gu N, et al. Co3O4 nanoparticles with multi-enzyme activities and their application in immunohistochemical assay. ACS Appl. Mater. Interfaces 6 (2014) 1959-1970.
[33] Ferretti S, Paynter S, Russell DA, Sapsford KE, Richardson DJ. Self-assembled monolayers: a versatile tool for the formulation of bio-surfaces. TRAC-Trend Anal. Chem. 19 (2000) 530-540.
[34] Feng L, Gao M, Tao D, Chen Q, Wang H, Dong Z, et al. Cisplatin-Prodrug-Constructed Liposomes as a Versatile Theranostic Nanoplatform for Bimodal Imaging Guided Combination Cancer Therapy. Adv. Funct. Mater. 26 (2016) 2207-2217.
[35] Torchilin VP. Recent advances with liposomes as pharmaceutical carriers. Nat. Rev. Drug

Discov. 4 (2005)145-160.
[36] Miranda D, Carter K, Luo DD, Shao S, Geng JM, Li CN, et al. Multifunctional Liposomes for Image-Guided Intratumoral Chemo-Phototherapy. Adv. Healthcare Mater. 6 (2017) 9-17
[37] Weber J, Beard PC, Bohndiek SE. Contrast agents for molecular photoacoustic imaging. Nature Methods 13 (2016) 639-650.
[38] Lee C, Kim J, Zhang YM, Jeon M, Liu CB, Song L, et al. Dual-color photoacoustic lymph node imaging using nanoformulated naphthalocyanines. Biomaterials 73 (2015)142-148.
[39] Zhang YS, Yao J, Zhang C, Li L, Wang LV, Xia Y. Optical-Resolution Photoacoustic Microscopy for Volumetric and Spectral Analysis of Histological and Immunochemical Samples. Angew. Chem. Inter. Ed. 53 (2014) 8099-8103.
[40] Cheng L, Wang C, Feng L, Yang K, Liu Z. Functional Nanomaterials for Phototherapies of Cancer. Chem. Rev. 114 (2014) 10869-10939.
[41] Chiang PH, Fang FM, Jong WC, Yu TJ, Chuang YC, Wang HJ. High-dose rate iridium-192 brachytherapy and external beam radiation therapy for prostate cancer with or without androgen ablation. Int. J. Urol. 11 (2004) 152-158.

Scheme 1. A scheme illustrating Ir@liposome as a sequentially acted, NIR-controllable theranostic nanozyme for cancer radiotherapy. In this process, Ir@liposome enables the precise *in vivo* PA imaging of tumors, and then efficient tumor endogenous H_2O_2 decomposition and hypoxia relief upon NIR laser induced mild photothermal heating. With the radio-sensitization capability of Ir as a high-Z element, greatly enhanced radiotherapy of tumors is further achieved with Ir@liposome.

Figure 1. Synthesis and Characterization of IrNCs and Ir@liposome. (a) A scheme showing the synthesis of IrNCs and the preparation of Ir@liposome. (b) TEM image and (c) XRD analysis of the as-prepared IrNCs. Inset in (b) is a high-resolution TEM image of IrNCs. (d) Oxygen generation profiles of IrNCs (5 μg mL^{-1}) in the 1 mM H_2O_2 solutions containing BSA at 0, 1, and 5 mg mL^{-1} measured using a portable dissolved oxygen meter. (e) TEM image of the as-prepared Ir@liposome. Inset in (e) is a high-resolution TEM image of encapsulated IrNCs. (f) DLS size distribution of IrNCs and Ir@liposome. (g) Oxygen generation profiles of Ir@liposome (Ir = 5 μg mL^{-1}) in the 1 mM H_2O_2 solutions containing BSA at 0, 1, and 5 mg mL^{-1}.

Figure 2. Temperature and NIR light Responsive Catalytic Activity of Ir@liposome. (a) UV-vis-NIR spectrum of IrNCs and Ir@liposome. Insets are the photographs of IrNCs (1) and Ir@liposome solutions (2). (b) Temperature change curves of Ir@liposome solution (10 □g mL^{-1}) under the irradiation of a 785-nm laser at 0.5, 1 and 1.5 W cm^{-2}. (c) Relative catalytic activities of both Ir@liposome and catalase towards H_2O_2 decomposition at varying temperatures for 1 min recorded by using the Góth method. (d) Oxygen generation profiles of Ir@liposome (Ir = 5 □g mL^{-1}) in the H_2O_2 solutions (1 mM) recorded at different temperature using a portable dissolved oxygen meter, respectively. (e) Oxygen generation profiles of H_2O_2 solutions (1 mM) in the presence or absence of Ir@liposome (Ir =10 μg mL^{-1}) under the exposure of the 785-nm laser at the power density of 1 W cm^{-2} using a portable dissolved oxygen meter. (f) A scheme showing the temperature and NIR light responsive oxygen generation via Ir@liposome mediated H_2O_2 decomposition.

Figure 3. *In vitro* Cell Viability and Radiosensitization Assays. (a) Relative viabilities of 4T1 cells after being incubated with Ir@liposome or Ir-GSH@liposome at varying concentrations for 24 h (n = 6). (b) Clonogenic survival assay of 4T1 cells treated with Ir@liposome or Ir-GSH@liposome under varied X-ray irradiation doses (n = 3). (c) γ-H_2AX immunofluorescence staining showing the DNA damage statuses of 4T1 cancer cells treated with Ir@liposome only, X-ray irradiation only, Ir-GSH@liposome plus X-ray irradiation, or Ir@liposome plus X-ray irradiation. The dose of X-ray was 6 Gy. The concentration of Ir was 50 μg mL^{-1}. (d) Semi-quantitative analysis of γ-H_2AX foci densities (γ-H_2AX foci/100 μm^2) in each treatment group shown in (c) with the Image J software (n = 100). *P* values were calculated by the Student's *t*-test: $^*P < 0.05$, $^{**}P < 0.01$.

Figure 4. *In vivo* PA Imaging and Pharmacokinetics Study. (a) Photoacoustic/ultrasound co-registered images of the subcutaneous Ir@liposome-Matrigel inclusions (50 μL) in mice at varying Ir concentration as indicated. (b) Linear correlation of PA signal intensities of Ir@liposome-Matrigel inclusions against corresponding Ir concentrations based on imaging data shown in (a). (c) In vivo PA imaging of 4T1 tumors bearing mice with i.v. injection of Ir@liposome recorded at different time intervals p.i. (d) Blood circulation profiles of Ir@liposome after i.v. injection. (e) Biodistribution profiles of Ir@liposome in 4T1 tumor bearing mice measured at 24 h p.i. The data were recorded by measuring Ir concentrations using ICP-MS. Error bars were based on three mice per group.

Figure 5. *In vivo* NIR-Enhanced Tumor Hypoxia Attenuation and Synergistic Cancer Radiotherapy. (a) *Ex vivo* immunofluorescence staining of tumor slices collected from mice with i.v. injection of Ir@liposome or Ir-GSH@liposome followed by exposure to a 785-nm laser for 20 min at 24 p.i. as indicated. The signals of hypoxia and nuclei were shown in green and blue, respectively. (b) Semi-quantitative analysis of the percentages of positive hypoxia areas in those slices with various treatments. (c) Tumor growth curves of mice after various treatments as indicated. V and V_o stand for the tumor volumes after and before the treatment, respectively. Error bars were based on five mice in each group. (d) *Ex vivo* TUNEL staining of tumor slices collected from mice from various groups at day 4 post various treatments. The signals of TUNEL and nuclei were shown in green and blue, respectively. Groups I, II, III, IV, V, VI and VII are same as those indicated in (c). Mice were injected with various agents at day 0, and subjected to NIR laser irradiation and / or X-ray exposure at day 1. P values were calculated by the Student's t-test: $^{*}P < 0.05$, $^{**}P < 0.01$.

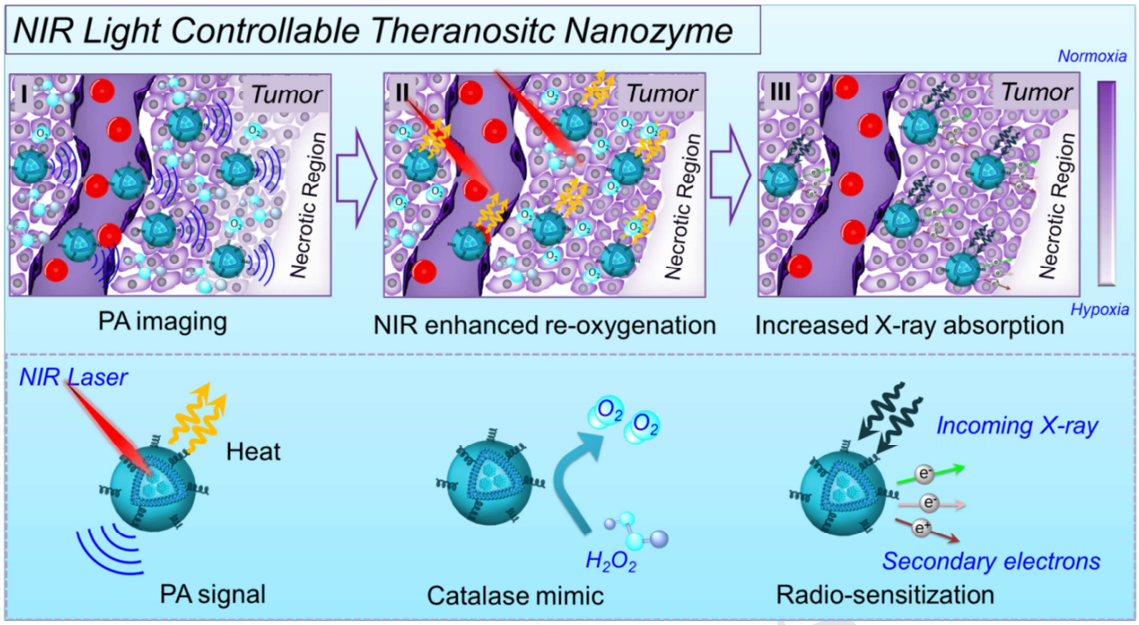

Scheme 1. A scheme illustrating Ir@liposome as a sequentially acted, NIR-controllable theranostic nanozyme for cancer radiotherapy. In this process, Ir@liposome enables the precise *in vivo* PA imaging of tumors, and then efficient tumor endogenous H_2O_2 decomposition and hypoxia relief upon NIR laser induced mild photothermal heating. With the radio-sensitization capability of Ir as a high-Z element, greatly enhanced radiotherapy of tumors is further achieved with Ir@liposome.

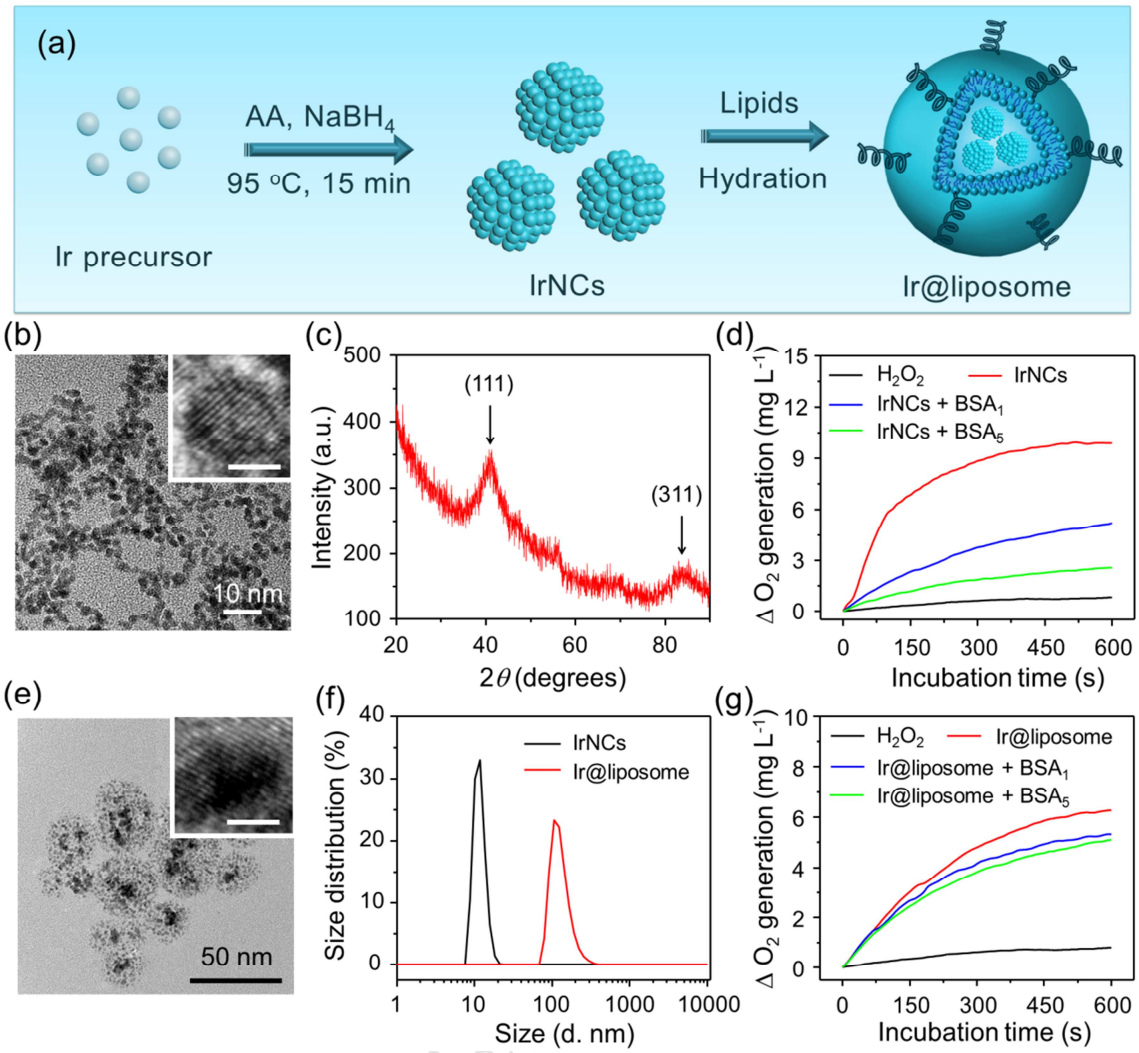

Figure 1. Synthesis and Characterization of IrNCs and Ir@liposome. (a) A scheme showing the synthesis of IrNCs and the preparation of Ir@liposome. (b) TEM image and (c) XRD analysis of the as-prepared IrNCs. Inset in (b) is a high-resolution TEM image of IrNCs. (d) Oxygen generation profiles of IrNCs (5 μg mL^{-1}) in the 1 mM H_2O_2 solutions containing BSA at 0, 1, and 5 mg mL^{-1} measured using a portable dissolved oxygen meter. (e) TEM image of the as-prepared Ir@liposome. Inset in (e) is a high-resolution TEM image of encapsulated IrNCs. (f) DLS size distribution of IrNCs and Ir@liposome. (g) Oxygen generation profiles of Ir@liposome (Ir = 5 μg mL^{-1}) in the 1 mM H_2O_2 solutions containing BSA at 0, 1, and 5 mg mL^{-1}.

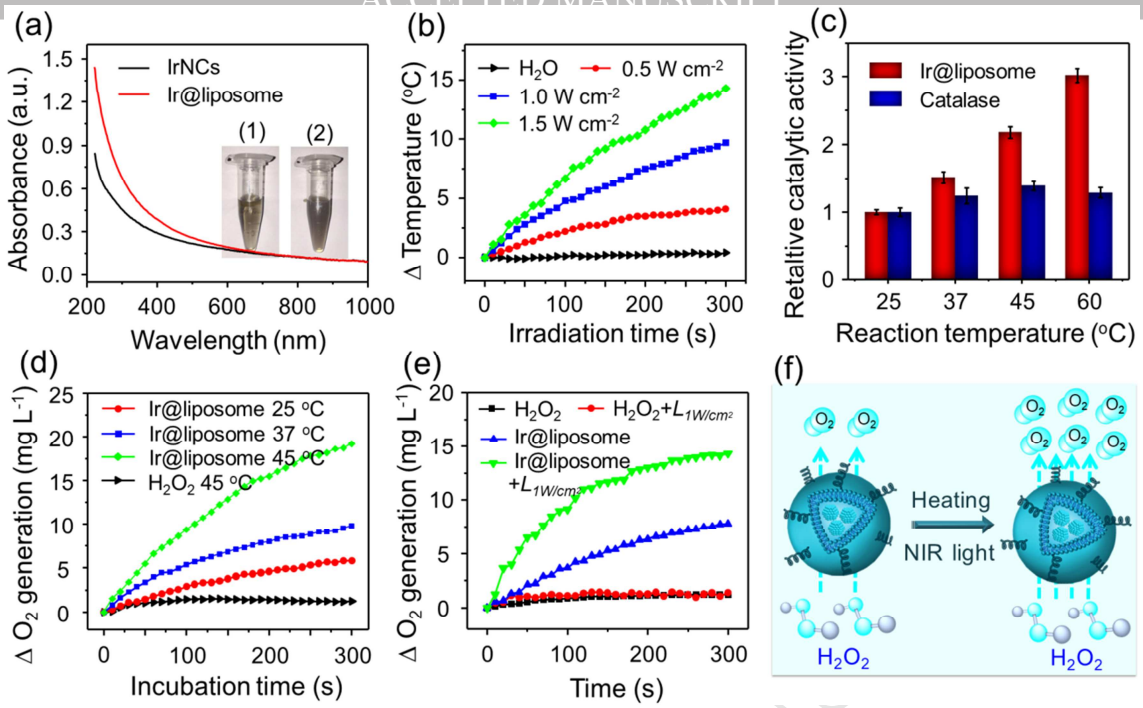

Figure 2. Temperature and NIR light Responsive Catalytic Activity of Ir@liposome. (a) UV-vis-NIR spectrum of IrNCs and Ir@liposome. Insets are the photographs of IrNCs (1) and Ir@liposome solutions (2). (b) Temperature change curves of Ir@liposome solution (10 □g mL^{-1}) under the irradiation of a 785-nm laser at 0.5, 1 and 1.5 W cm^{-2}. (c) Relative catalytic activities of both Ir@liposome and catalase towards H_2O_2 decomposition at varying temperatures for 1 min recorded by using the Góth method. (d) Oxygen generation profiles of Ir@liposome (Ir = 5 □g mL^{-1}) in the H_2O_2 solutions (1 mM) recorded at different temperature using a portable dissolved oxygen meter, respectively. (e) Oxygen generation profiles of H_2O_2 solutions (1 mM) in the presence or absence of Ir@liposome (Ir =10 μg mL^{-1}) under the exposure of the 785-nm laser at the power density of 1 W cm^{-2} using a portable dissolved oxygen meter. (f) A scheme showing the temperature and NIR light responsive oxygen generation via Ir@liposome mediated H_2O_2 decomposition.

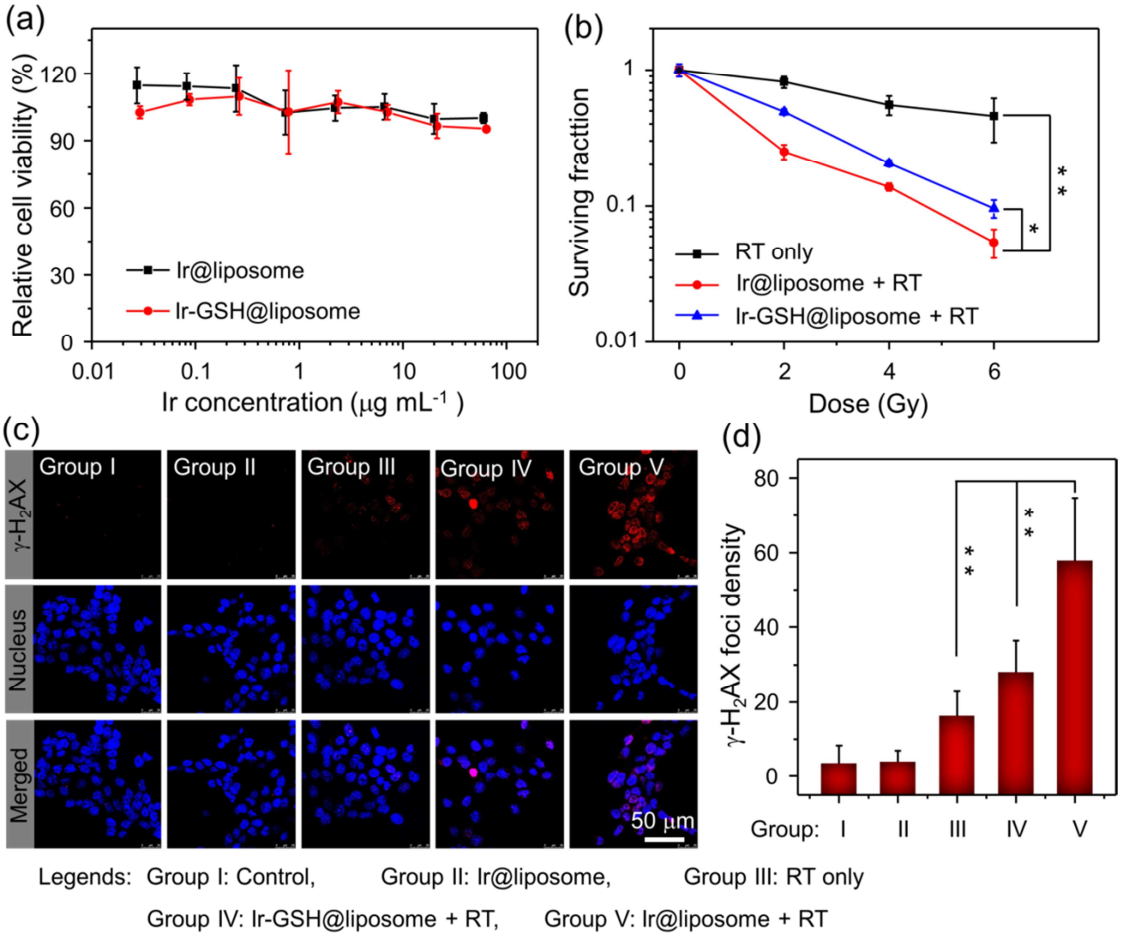

Figure 3. *In vitro* Cell Viability and Radiosensitization Assays. (a) Relative viabilities of 4T1 cells after being incubated with Ir@liposome or Ir-GSH@liposome at varying concentrations for 24 h (n = 6). (b) Clonogenic survival assay of 4T1 cells treated with Ir@liposome or Ir-GSH@liposome under varied X-ray irradiation doses (n = 3). (c) γ-H_2AX immunofluorescence staining showing the DNA damage statuses of 4T1 cancer cells treated with Ir@liposome only, X-ray irradiation only, Ir-GSH@liposome plus X-ray irradiation, or Ir@liposome plus X-ray irradiation. The dose of X-ray was 6 Gy. The concentration of Ir was 50 μg mL^{-1}. (d) Semi-quantitative analysis of γ-H_2AX foci densities (γ-H_2AX foci/100 μm^2) in each treatment group shown in (c) with the Image J software (n = 100). *P* values were calculated by the Student's *t*-test: **P* < 0.05, ***P* < 0.01.

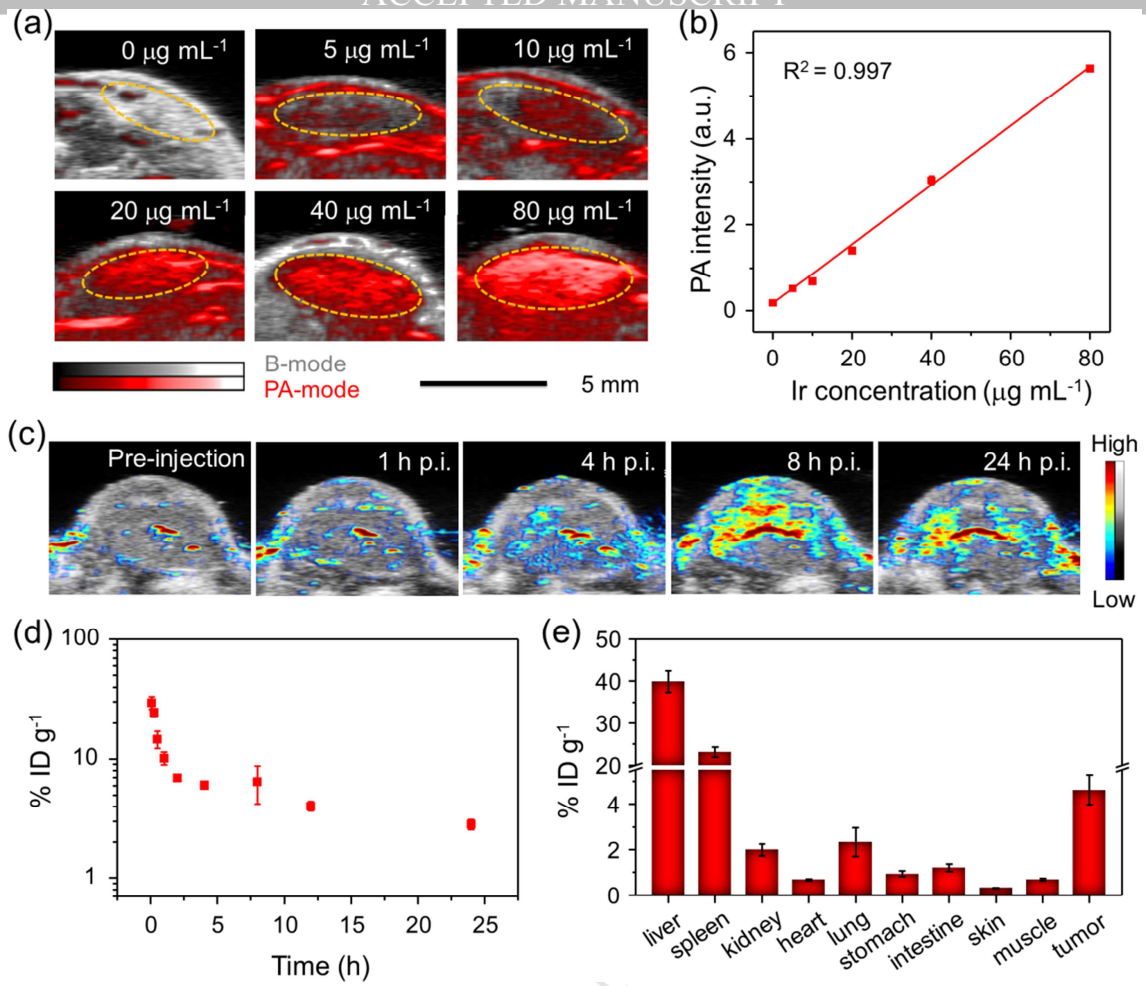

Figure 4. *In vivo* PA Imaging and Pharmacokinetics Study. (a) Photoacoustic/ultrasound co-registered images of the subcutaneous Ir@liposome-Matrigel inclusions (50 μL) in mice at varying Ir concentration as indicated. (b) Linear correlation of PA signal intensities of Ir@liposome-Matrigel inclusions against corresponding Ir concentrations based on imaging data shown in (a). (c) In vivo PA imaging of 4T1 tumors bearing mice with i.v. injection of Ir@liposome recorded at different time intervals p.i. (d) Blood circulation profiles of Ir@liposome after i.v. injection. (e) Biodistribution profiles of Ir@liposome in 4T1 tumor bearing mice measured at 24 h p.i. The data were recorded by measuring Ir concentrations using ICP-MS. Error bars were based on three mice per group.

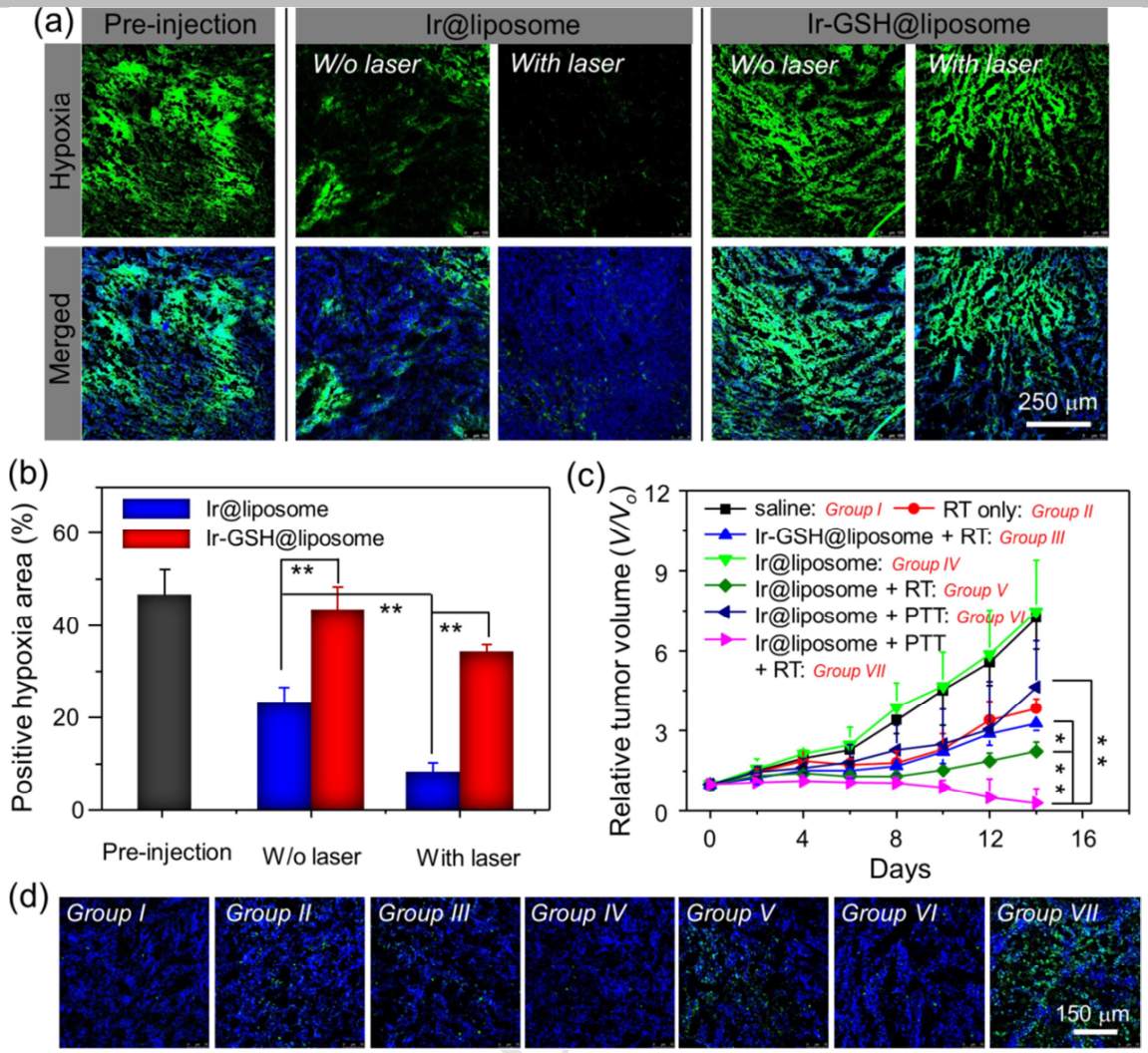

Figure 5. *In vivo* NIR-Enhanced Tumor Hypoxia Attenuation and Synergistic Cancer Radiotherapy. (a) *Ex vivo* immunofluorescence staining of tumor slices collected from mice with i.v. injection of Ir@liposome or Ir-GSH@liposome followed by exposure to a 785-nm laser for 20 min at 24 p.i. as indicated. The signals of hypoxia and nuclei were shown in green and blue, respectively. (b) Semi-quantitative analysis of the percentages of positive hypoxia areas in those slices with various treatments. (c) Tumor growth curves of mice after various treatments as indicated. V and V_o stand for the tumor volumes after and before the treatment, respectively. Error bars were based on five mice in each group. (d) *Ex vivo* TUNEL staining of tumor slices collected from mice from various groups at day 4 post various treatments. The signals of TUNEL and nuclei were shown in green and blue, respectively. Groups I, II, III, IV, V, VI and VII are same as those indicated in (c). Mice were injected with various agents at day 0, and subjected to NIR laser irradiation and / or X-ray exposure at day 1. P values were calculated by the Student's t-test: $^*P < 0.05$, $^{**}P < 0.01$.